Accepted version, published as Danielson *et al.*, Phys. Rev. A **108**, 032801 (2023)

Positron Binding to Alkane Molecules

J. R. Danielson[1],* S. Ghosh[2], E. Arthur-Baidoo[1], D. R. Witteman[1], and C. M. Surko[1]
[1]*Physics Department, University of California San Diego, La Jolla, CA 92093, USA and*
[2]*Division of Mathematical and Physical Sciences,*
Ahmedabad University, Navrangpura, Ahmedabad 380009, Gujarat, India
(Dated: September 18, 2023)

Measurements are presented for the low-energy positron annihilation spectra of the alkane molecules propane through octane. The downshift of the vibrational Feshbach resonances of the infrared-active C-H stretch vibrational modes is used to obtain updated values for the positron-molecule binding energies for these molecules. These binding energies correct previously reported values which had systematic energy shifts due to several small, but significant errors in the analyses. Once these energy shifts are corrected, the old and new measured spectra are in good agreement. This updated analysis procedure is applied to other previously measured alkanes, providing updated binding energies for these molecules. The resulting data are shown to be in good agreement with a recent model-potential calculation and solve issues regarding the interpretation of previous measurements.

I. INTRODUCTION

Low-energy positron annihilation in most molecules is dominated by vibrational Feshbach resonances (VFR). Measurement of the downshifts in energy of these resonances relative to the molecular vibrational modes provides a direct measurement of the positron-molecule binding energy [1, 2]. The chain alkane molecular bonds are fully saturated (i.e., with all single C-H and C-C bonds), and have either no, or very small dipole moments. They have molecular polarizabilities that increase approximately linearly with the number of carbon atoms [3]. Historically, the exponential increase in the annihilation rate for thermal positrons with increasing molecular size provided early evidence for positron binding [4–6].

Later, use of a buffer-gas-trap (BGT) based positron beam led to the observation of distinct VFR, and the resulting measurements showed a linear increase in the positron binding energy with molecular size [3, 7–9]. Understanding this dependence and providing accurate positron binding energies for large molecules has been a significant challenge for theory [10]. Thus, alkane molecules provide an important test case for experiment and theory in investigating positron binding to molecules and the associated phenomenon of Feshbach-resonant annihilation.

Presented here are updated annihilation-spectral measurements for six chain alkanes propane through octane using a room temperature, BGT-based positron beam [7, 8, 11–13]. Using the measured beam parameters, fits to the spectra in the region of the high-energy C-H stretch modes are used to measure positron-molecule binding energies ε_B with improved accuracy. A systematic shift in the energy scale of older measurements is identified. After correcting for this shift, there is good agreement between previous and newly measured spectra, and enables more accurate ε_B values for other molecules studied previously.

The absolute spectral amplitudes of the data sets are also compared and show good agreement even though they were measured with somewhat different apparatus and beam parameters. For the largest molecules, the effect of counting errors on the magnitude of the annihilation is identified and corrected in the new measurements. Although these errors can have a significant impact on the measured annihilation rates, they are shown to have only a relatively small effect on the measured ε_B values.

The revised analysis procedures are used to determine the binding energies for all other alkane molecules studied previously. This yields a new estimate of ε_B for ethane that resolves a mystery associated with the previous measurement [7]. Updated ε_B values for the larger alkanes (dodecane, tetradecane, and hexadecane) are also obtained, including new estimates for the previously measured binding energies of the second bound states observed in these molecules. Also considered for comparison are data for the related molecular species, cycloalkanes and alkane isomers. For brevity, in this paper, the latter are referred to by those designations, while the chain alkanes are simply called alkanes.

These new and corrected binding energy values are compared with the recent model-potential calculations by Swann and Gribakin [15, 16]. They show good agreement with the measurements, including the observation of a departure from a linear trend in ε_B with increasing molecular size. More generally, these model-based calculations for larger

* jrdanielson@ucsd.edu

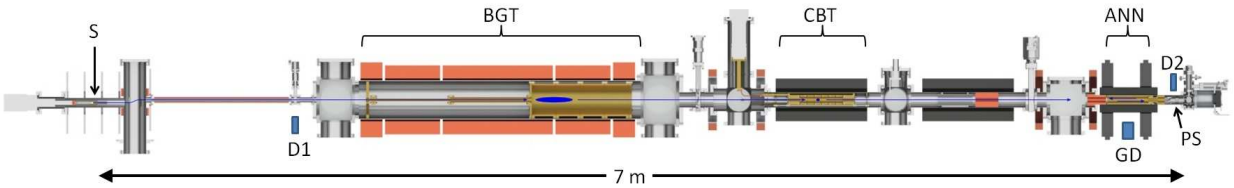

FIG. 1. Schematic diagram of the positron beam line. It consists of a positron source S; buffer gas trap, BGT; cryo-beam trap, CBT; annihilation cell, ANN; calibrated gamma ray detector, GD; and phosphor screen, PS (for beam characterization). D1 and D2 are gamma detectors for beam diagnostics. See ref. [14].

molecules have been complemented by *ab initio* calculations for smaller molecules and other, more precise experimental measurements, resulting in much improved confidence in the methodologies and important physical insights [15, 17–21]. Reference [18] elucidates the important role of electron-positron correlations in positron-molecule binding energies, which is found to be critical, for example, in providing accurate ε_B values for non-polar and weakly polar molecules and aromatic molecules with π bonds.

The remainder of the paper is organized as follows: Section II describes the experimental apparatus and procedures. Section III describes previous and new data analysis procedures, and Section IV describes the new measurements for propane through octane. Section V compares the old and new measurements, including the identification of a significant systematic energy shift. Also discussed is the correction of counting errors in the peak annihilation amplitudes which is important for the larger molecules studied. Section VI discusses previous measurements for other alkanes and provides corrected ε_B values. The new and corrected data sets are compared to the predictions of recent model-potential calculations [15, 16]. Section VII presents a comparison of binding energies for alkane rings, chains and isomers. Section VIII summarizes key results and presents a set of concluding remarks.

II. EXPERIMENTAL APPARATUS AND PROCEDURES

The experiments for which new measurements are presented here use the room temperature BGT described in Ref. [7], but with a number of modifications, as discussed below. Differences between this and the earlier configuration that affect the systematics of the analysis are described when comparing data sets in Section V. The beamline, which is shown in Fig. 1, uses a ^{22}Na positron source and a solid-Ne moderator to provide the source of low-energy positrons. Positrons are magnetically guided through the beam line using different strength magnetic fields and electrostatic potentials. Positrons from the moderator enter a three-stage, room-temperature BGT [22]. Here, they scatter inelastically with N_2 and CF_4 to become trapped and cooled to the ambient temperature (300 K) in the third-stage electrostatic potential well [23]. The trapped charge cloud has a typical diameter of ~ 10 mm and a length of ≤ 50 mm [24].

The beam is formed by adiabatically ramping the bottom of the potential well to a voltage higher than that of the exit gate [11, 24]. The beam thus formed has a mean energy just slightly higher than the exit gate as measured using a retarding potential analyzer (RPA) downstream. For the experiments described here, the measured parallel energy distribution is approximately Gaussian with a standard deviation $\sigma \sim 7$ - 9 meV (i.e., FWHM ~ 16 - 22 meV). This energy spread is determined mostly by the temporal dynamics of the ejection ramp and depends only weakly on the initial positron temperature [24, 25].

For the measurements presented here, there was a magnetic minimum near the exit of the third stage of the trap due to a partial short in the BGT magnet [24]. As the trap potential is increased during the ramp, the axial center of the electrostatic well moves ~ 5 cm, and this decreases the average magnetic field by about 20% during beam ejection. Due to the adiabatic invariant associated with the magnetized positrons, this decreases the perpendicular energy (mean and spread) of the particles from $\sim$ 25 to $\sim$ 20 meV. The excess energy goes into the parallel energy of the particles. However, because the parallel energy spread is dominated by the time dependence of the voltage ramp, it is not changed appreciably (cf. Ref [24]). Since the position of the annihilation resonance is set by the total energy distribution of the beam, precise knowledge of these energy spreads is necessary for accurate fits to the measured resonances [1].

A measurement of the parallel energy distribution of the beam is shown in Fig. 2 using the annihilation cell as an RPA. In Fig. 2(a), the number of positrons passing the RPA is shown versus the ap-

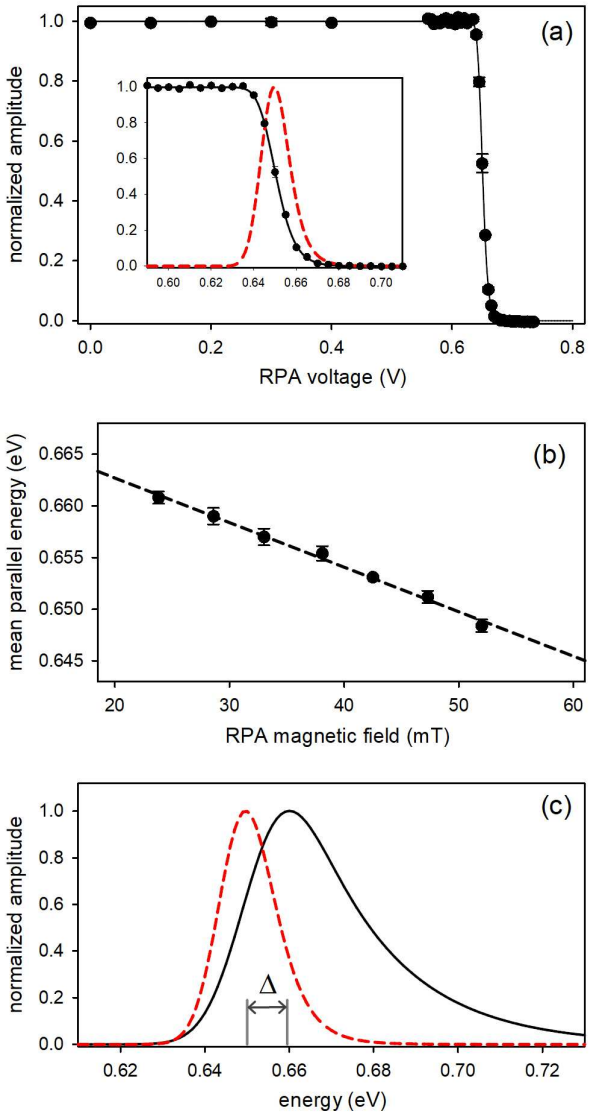

FIG. 2. (a) Example of an RPA measurement of the parallel energy distribution of the positron beam for the same magnetic field of 47 mT at the BGT and analyzer. The inset shows the region near the cutoff in greater detail. The red dashed line shows the normalized derivative of the curve, which is the approximately Gaussian, parallel energy distribution of the beam. (b) The mean parallel energy of the beam as a function of the magnetic field at the RPA. The slope is a measure of the mean perpendicular energy, $\langle E_\perp \rangle = 20 \pm 2$ meV [24]. (c) Comparison of the total energy distribution (solid line) to the parallel energy distribution (dashed line) from the inset in (a). The shift of the peak is $\Delta = 9$ meV. See text for details.

plied RPA voltage. The inset shows the cutoff region in detail, where the dashed line is the (arbitrarily scaled) derivative of the cumulative curve. It shows the measured Gaussian parallel energy distribution, with a mean energy of 651 ± 1 meV and standard deviation $\sigma = 8 \pm 1$ meV (FWHM $\sim$ 18 meV). The perpendicular energy is determined by measuring the mean parallel energy as a function of the RPA magnetic field [14, 24]. The results are shown in Fig. 2(b), where the slope corresponds to $\langle E_\perp \rangle = 20 \pm 2$ meV. Combining the measured parallel distribution with the measured perpendicular energy spread yields the exponentially modified Gaussian (EMG) distribution for total energy distribution which is shown in Fig. 2(c). For these data, the shift between the mean parallel energy and the peak of the total distribution is $\Delta = 9$ meV, and the FWHM of the total distribution is approximately 34 meV. This is the highest-quality beam obtained to date from the room-temperature BGT.

The annihilation gas cell (ANN in Fig. 1) is located at the end of the beam line with several other experimental regions in between which are not used in the present experiments. Although the magnetic field varies by a factor of five in the beam line, the low-energy particles are guided adiabatically in all regions [14, 26]. Thus, if the magnetic field in the annihilation region is the same as that at the *exit* of the BGT, both the parallel and perpendicular particle distributions will be the same at both locations, and the EMG for the total energy distribution is known for positrons interacting with the test gas.

The positrons propagate downstream to the annihilation region where a 26 cm long gas cell is used to set the mean parallel energy of the positrons. During annihilation measurements, an isolated electrode after the annihilation cell is biased to 6 V to reflect the beam back toward the BGT. Upon returning to the BGT, the positrons are reflected and once again return to the annihilation cell. This can continue for hundreds of bounces. Here, a single bounce is defined as one round trip through the detector region and back to the BGT. The bounce time is typically $\sim 16\mu$s, with a positron pulse FWHM $\sim 3\mu$s.

As the positrons transit the annihilation cell, they interact with the test gas, and annihilation γ rays are recorded from an approximately 10 cm FWHM long field-of-view at the axial center of the gas cell using a single CsI gamma detector (GD in Fig. 1). The annihilation signal for octane, measured on an oscilloscope, is shown in Fig. 3, averaged over 20 pulses. The resulting average number of γ in the first bounce is 17 ± 1. The Gaussian pulse has a FWHM $\approx 5\mu$s and corresponds to an average integrated area of 1.3 $\pm$0.1 V-μs per γ. The total width is a combination of the detector and the reflecting positron pulse, resulting in a typical FWHM $\sim 6\mu$s (c.f. Fig. 3). Although many bounces can occur, annihilation radiation is typically recorded only during

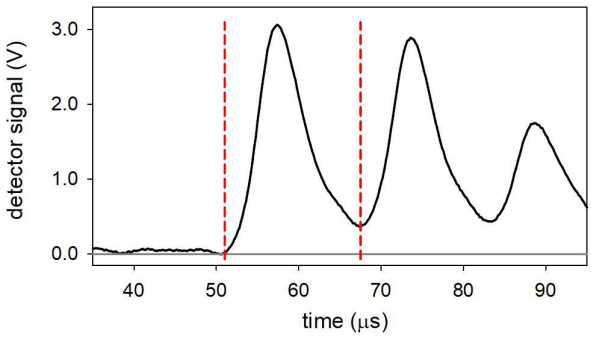

FIG. 3. Averaged annihilation gamma-ray signal for 20 beam pulses for octane at a pressure of 10 μtorr, with $\langle E_{||} \rangle = 0.2$ eV. Three bounces of the positron pulse through the annihilation cell are visible. Only data for the first bounce (marked by the dashed lines) are used in the analysis of the new data presented here.

the first 3 - 5 bounces. For the new data presented here, only the first bounce is used (marked by the dashed lines in Fig. 3) to avoid multiple scattering and other deleterious effects.

The annihilation cell and most of the other surfaces in view of the positron beam are coated with colloidal graphite to minimize potential variations due to charging of the electrodes. This is effective even after repeated exposure to a variety of test gases and periodic baking of the system. Using this procedure, the measured mean energy of the positron beam typically varies by less than 2 meV over the course of 12 h, which is the maximum duration of a typical experiment.

Earlier experiments used transport energies $\sim 3-5$ eV and a shorter beam-line, so the bouncing pulses of positrons overlapped, and one was forced to estimate the number of bounces during the counting time window [7]. Since then, a "cryo-beam trap" (CBT, cf. Fig. 1) was added to the beam line [27] which increased the total beam-line length by about 1 meter. This has the effect of increasing the time of flight of the positrons from the BGT to the annihilation region. Use of the longer path length and a considerably lower transport energy ($0.6-1$ eV) enables the ability to distinguish *individual* bounces of the beam and thus to determine the number of detected γ rays per bounce with greater certainty. An example of this for octane is shown in Fig. 3, where the first three bounces are easily distinguished. Importantly, it was discovered that the subsequent bounces that return to the BGT are slightly "lifted" in energy (by several meV or more) with each successive bounce [28]. This results in a broader energy spread when multiple bounces are summed, and likely contributed to some broadening of the peaks in the older data [7].

In contrast to using only the integrated signal from the first bounce, the previous experiments used a single-channel analyzer (SCA) to measure single annihilations during a fixed time window, typically 15 μsec, that included approximately $2-5$ bounces of the beam [7]. Because of the broad detector response and higher transport energy, the bounce time was faster than the detector response. Thus, multiple γ in a single bounce (or from subsequent bounces) overlapped enough to push the signal amplitude outside the SCA window and thus led to a loss of counts. As compared to the new experimental data, the previous measurements appear to have suffered from counting errors, up to 30% at the larger annihilation rates, primarily near the peaks of the C-H stretch resonances.

With both integrated-signal and SCA detection techniques, the annihilation counts N_c are converted to an annihilation cross-section using the test-gas pressure to get the molecule density n_m, the positron number in a pulse N_p, the calibrated detector efficiency η_D, and the detector length L_D. At each energy, the normalized annihilation rate, $Z_{\rm eff}(E)$, is given by [7]

$$Z_{\rm eff}(E_{||}) = \frac{N_c(E_{||})}{2N_p\eta_{\rm D}L_{\rm D}n_m}\frac{v(E_{||})}{\pi r_0^2 c}, \qquad (1)$$

where $v(E_{||})$ is the average particle velocity, r_0 is the classical radius of the electron, and c is the speed of light. The factor of 2 in the denominator accounts for the two trips through the annihilation cell per bounce.

III. DATA ANALYSIS

The data are displayed below as a function of the mean parallel energy of the beam particles. However, the resonant annihilation signal is a function of the *total* particle energy, and thus a convolution of the total energy distribution at each parallel energy. Due to this convolution, there is a shift between the peak of the total energy distribution and the mean parallel energy, as shown in Fig. 2(c). This shift needs to be included to obtain accurate values of $\varepsilon_{\rm B}$.

In the new analysis for which results are presented here, the measured EMG distribution is convolved with a δ function located at each IR-active fundamental mode, downshifted by $\varepsilon_{\rm B}$, to fit the annihilation spectrum as a function of mean parallel energy, and thus the correct shift is included. However, the need for the EMG distribution was not recognized at

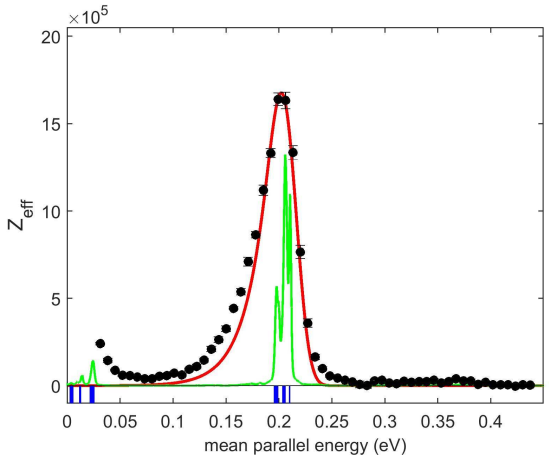

FIG. 4. Normalized annihilation rate $Z_{\rm eff}$ for octane vs mean parallel energy. Vertical blue bars show the locations of the downshifted vibrational modes [29]. The solid green line is the downshifted and arbitrary scaled IR spectrum [30]. The solid red line shows the fit to the C-H modes with the result that $\varepsilon_{\rm B} = 147 \pm 3$ meV.

the time of the previous experiments, so an approximate procedure was used to account for the perpendicular components of the particle energy. This led to small, but significant errors in the binding energy which we correct here (cf. Sec. V).

Shown in Fig. 4 is the newly measured spectrum of octane, where $Z_{\rm eff}$ is plotted vs the mean parallel energy from 0.04 eV to 0.45 eV. This spectrum was taken using the integrated-signal technique at a test gas pressure of 10 μtorr and $\sim 40,000$ positrons per pulse. The linearity of the signal as a function of pressure was verified by measurements at several pressures. Error bars are statistical, based on multiple scans over the energy range.

The relative error across the spectrum is purely statistical and is usually better than $\pm 5\%$. However, the total, absolute uncertainty of these measurements is higher. It is dominated by the uncertainty in the test-gas pressure. Although the monometer measurement is better than ± 0.5 μtorr in the range 5 - 50μtorr, the pressure is measured at the high-pressure end of the annihilation cell, and there is an approximately 40% pressure drop due to the gas conductance through the 26 cm long cell. The drop across the field of view is less, only $\pm 7\%$, and so this is not expected to cause a problem but the average pressure at the center of the cell needed to be calibrated. This calibration was done using a second monometer placed at the center of the cell, resulting in a combined overall estimated uncertainty of $\sim 10\%$.

To fit the C-H stretch resonance, each IR-active vibrational mode is treated as a δ function and convolved with the EMG using the measured beam parameters. The positron coupling is assumed to be the same for all modes and in the limit where the annihilation width is small compared to the dipole excitation width [1, 2]. The resonance from all modes are then summed to give a single resonance peak with a width that is a combination of the beam parameters and the spread in energy of the vibrational modes. The binding energy, $\varepsilon_{\rm B}$, and peak amplitude enhancement are varied independently to obtain a least-squares best fit to the data.

The low-energy side of the peaks is known to be broadened due to effects beyond the fundamental modes [31, 32]. Thus, no attempt was made to fit the entire spectrum, since the origin of the annihilation near, but below the C-H stretch peak is not presently understood. For both new and corrected spectra, only data points near the peak and on the high-energy edge of the resonance are used in the analysis. For the current data, the points are typically spaced by 10 meV, leading to the use of 6 - 8 data points (spread over 50 - 70 meV). This is enough to constrain the curve and determine the experimental value of $\varepsilon_{\rm B}$ [21, 31]. The example of octane is shown in Fig. 4. The solid green line shows the downshifted IR spectrum [30], arbitrarily scaled. Only the 9 IR-active, high-energy C-H modes (blue vertical lines, spread over 14 meV, near 0.2 eV) are used to obtain $\varepsilon_{\rm B}$. The fit is shown as the solid red line and corresponds to $\varepsilon_{\rm B} = 146.9 \pm 0.4$ meV with reduced $\chi^2 = 0.9$. If only a single mode were used, the value for $\varepsilon_{\rm B}$ would differ by up to 5 meV, depending on the mode, however, every choice leads to reduced $\chi^2 > 10$, and thus a model with only a single resonant mode is excluded. As discussed below, there is extra uncertainty associated with other assumptions in the model, so the final measurement for octane is $\varepsilon_{\rm B} = 147 \pm 3$ meV.

These same procedures were used for all of the molecules in the current study. The requirements for this analysis include knowledge of the energies of all the IR-active vibrational modes and measurement of the beam parameters. For the new data sets, $\sigma_{||}$ is in the range of 7 - 9 meV, and $\sigma_{\perp}$ is approximately $20\pm$ 2 meV (cf. Fig. 2). For comparison, in the older data sets discussed below, $\sigma_{||}$ was $\sim$ 11 - 13 meV, and $\sigma_{\perp}$ was approximately 25 meV [7]. While the beam used for the older measurements was somewhat broader than the current beam, at least for the alkanes, the spread in the energies of the C-H modes broadens the resonances so the difference is small. However, due to the difference in perpendicular energy, there is a $\sim$ 1 meV change in Δ, which needs to be included for a correct comparison.

There are two sources of uncertainty in this analysis. The first is the use of only a few data points in

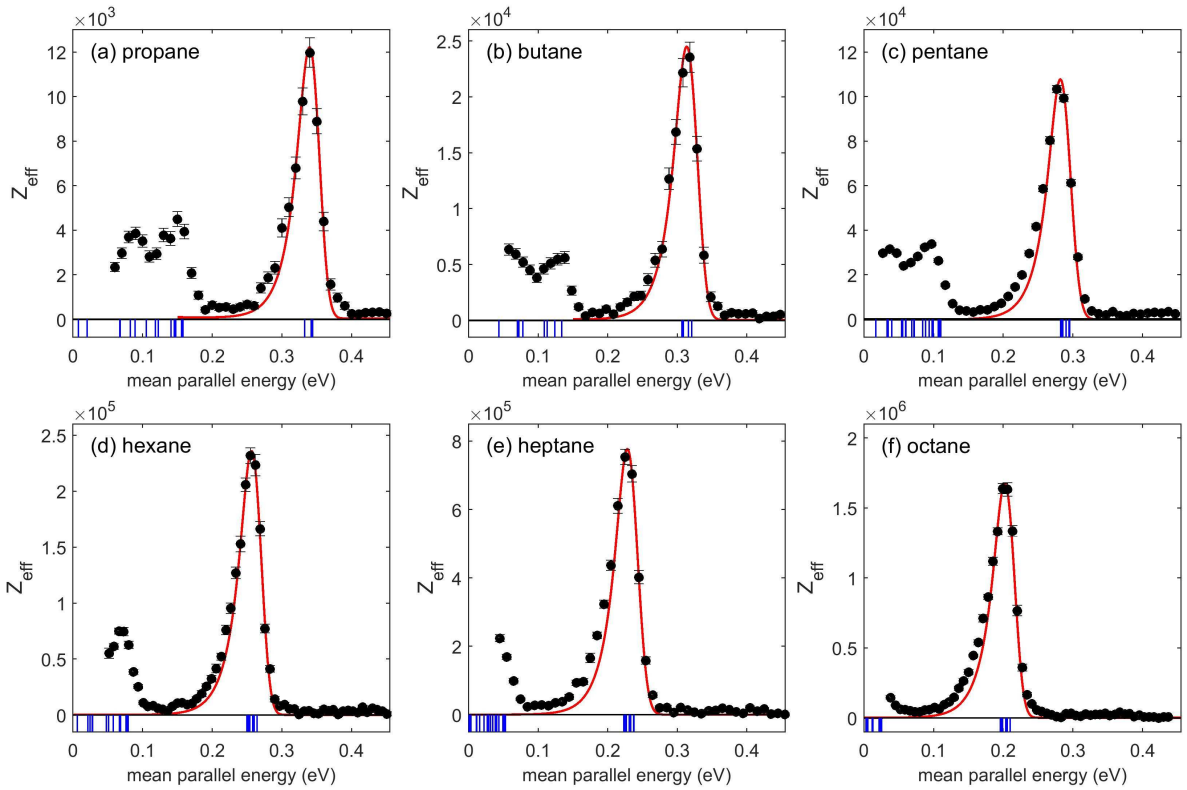

FIG. 5. New $Z_{\rm eff}$ measurements for the linear alkane molecules propane through octane. The vertical blue bars show the downshifted locations of the IR-active fundamental vibrations, and the solid red lines are fits to the C-H stretch peaks. Data in (a) and (b) use the SCA detection technique, and (c) - (f) use the integrated-signal technique, discussed in the text.

the fit. The choice of which points to use is somewhat arbitray. It is hard to ascertain quantitatively the exact impact of this assumption without higher resolution data. However, comparison of the spectra for cyclopentane in Ref. [32] between the lower resolution BGT and higher resolution CBT, showed that they yield the same $\varepsilon_{\rm B}$. Thus, this analysis is believed to be adequate for the alkane data presented here but could be investigated further when higher resolution spectra are available.

The second source of uncertainty is the assumption of a single amplitude factor for *all* IR-active C-H modes. The peak of the convolution is located near the average mode energy, weighted by the mode degeneracy factors, with a width that depends on the spread of the modes. If the different types of modes (e.g. associated with methyl, CH_3, vs. methylene, CH_2 groups) have different couplings to the incident positron, then the location of the peak will change, leading to a change in $\varepsilon_{\rm B}$. The most extreme case would be to have all the coupling in a single mode, which could change $\varepsilon_{\rm B}$ by up to ± 5 meV. This would also change the width of the convolved peak and lead to significantly larger χ^2, and thus is excluded. However, more modest changes in the couplings across the modes are possible which would influence the final fit to $\varepsilon_{\rm B}$. With these assumptions, the typical total uncertainty of the new measurements is estimated to be $\sim \pm 3$ meV unless otherwise stated.

IV. NEW MEASUREMENTS

The results for the six chain alkanes, propane through octane, are shown in Fig. 5, where the data for $Z_{\rm eff}$ are shown as a function of the mean parallel energy. A value for $\varepsilon_{\rm B}$ is found for each molecule from the fit to the C-H peak. The results are summarized in Table I, along with relevant molecular parameters. These fits do a reasonably good job capturing the C-H peak and high-energy edge for all of the molecules studied. For the alkanes, there is typically a spread of the C-H stretch mode energies of about 10 - 15 meV [29]. Although smaller than the energy width of the beam, the convolution with the modes broadens the peak by 3 - 5 meV relative to that for a single mode, and is necessary to obtain the best fit with the data.

TABLE I. New and corrected (*) measurements of ε_B (with uncertainties) are compared to previously reported values ε_{B1} (from Ref. [7–9] unless otherwise noted). Also included are model-potential calculations ε_B(SG), where SG represents the Swann-Gribakin-Model results [15], and thermally averaged conformer calculations $\varepsilon_B(300)$ assuming a molecular gas temperature of 300 K [16]. Also shown are the molecular polarizability α and the ionization potential E_i values from [33]. Values marked * are those obtained after correcting the energy scale of the previous measurements and using the fit procedure described in the text.

Molecule		ε_B [meV]	ε_{B1} [meV]	ε_B(SG) [meV]	$\varepsilon_B(300)$ [meV]	α [Å^3]	E_i [eV]
Chain alkanes							
ethane	C_2H_6	3*±3	< 0	-2	–	4.4	11.5
propane	C_3H_8	16 ±3	10	4	–	6.3	11.1
butane	C_4H_{10}	37 ±3	35	26	–	8.1	10.5
pentane	C_5H_{12}	67 ±4	60	56	–	10.0	10.3
hexane	C_6H_{14}	93 ±3	80	87	–	11.8	10.1
heptane	C_7H_{16}	118 ±3	105	117	121	13.7	9.9
octane	C_8H_{18}	147 ±3	115	144	–	15.5	9.8
nonane	C_9H_{20}	178*±8	145	168	–	17.4	9.7
decane	$C_{10}H_{22}$	193*±10	170[1]	189	198	19.2	9.7
dodecane	$C_{12}H_{26}$	225*±10	220	222	243	22.8	9.8
tetradecane	$C_{14}H_{30}$	265*±10	260[2]	246	269	26.6	9.7
hexadecane	$C_{16}H_{34}$	295*±10	310[2]	264	292	30.3	9.6
2nd bound states							
dodecane	$C_{12}H_{26}$	5*±4	> 0	10	–	22.8	9.8
tetradecane	$C_{14}H_{30}$	45*±8	50[2]	55	42	26.6	9.7
hexadecane	$C_{16}H_{34}$	75*±12	100[2]	96	83	30.3	9.6
Cycloalkanes							
cyclopropane	C_3H_6	16* ±6	10[2]	1	–	5.7	9.9
cyclobutane	C_4H_8	–	–	13	–	7.3	9.8
cyclopentane[3]	C_5H_{10}	47 ±4	–	41	–	9.1	10.3
cyclohexane	C_6H_{12}	82 ±4	80[2]	76	–	11.0	9.9
cycloheptane	C_7H_{14}	104 ±4	–	118	–	12.8	10.0
cyclooctane[3]	C_8H_{16}	128 ±4	–	172	–	14.6	9.8
cyclononane	C_9H_{18}	–	–	219	–	16.3	–
cyclodecane	$C_{10}H_{20}$	–	–	260	–	18.5	9.7
Alkane isomers							
isobutane[4]	C_4H_{10}	41 ±3	–	–	–	8.0	10.6
isopentane	C_5H_{12}	65* ±6	60[3]	59	–	10.0	10.3
2,3-dimethylbutane[4]	C_6H_{14}	93 ±3	–	–	–	11.8	10.0

[1]Data from Ref. [34].
[2]Data from Ref. [8].
[3]Data from Ref. [32].
[4]Data from Ref. [20].

V. COMPARISON OF NEW AND OLDER DATA

As discussed above, there are three differences in the experimental apparatus for the data presented here compared with previous data. First, the use of a longer beam-line and lower beam transport energy means that each individual bounce can be distinguished. Second, an integrated detector scheme is used instead of pulse counting with an SCA. Third, the magnetic field profile is different. Now there is a minimum near the exit of the BGT, whereas previously it was uniform (to ±2%) through all stages of the BGT. But the magnetic field used at the annihilation cell was previously 2/3 the value at the BGT. Beyond those changes, the method of setting the energy scale and the use of the proper energy distribution ultimately set the accuracy of the measurements of ε_B.

For the previous experiments, the mean perpendicular energy exiting the trap was 25 meV; from the drop in magnetic field, the mean perpendicular energy at the annihilation cell was only 16 meV. To account for this difference, 16 meV was added to the measured mean parallel energy at the annihilation cell, and the annihilation data were plotted vs mean *total* energy [7, 8]. Then, to obtain ε_B, the shift of the peak of the annihilation was compared

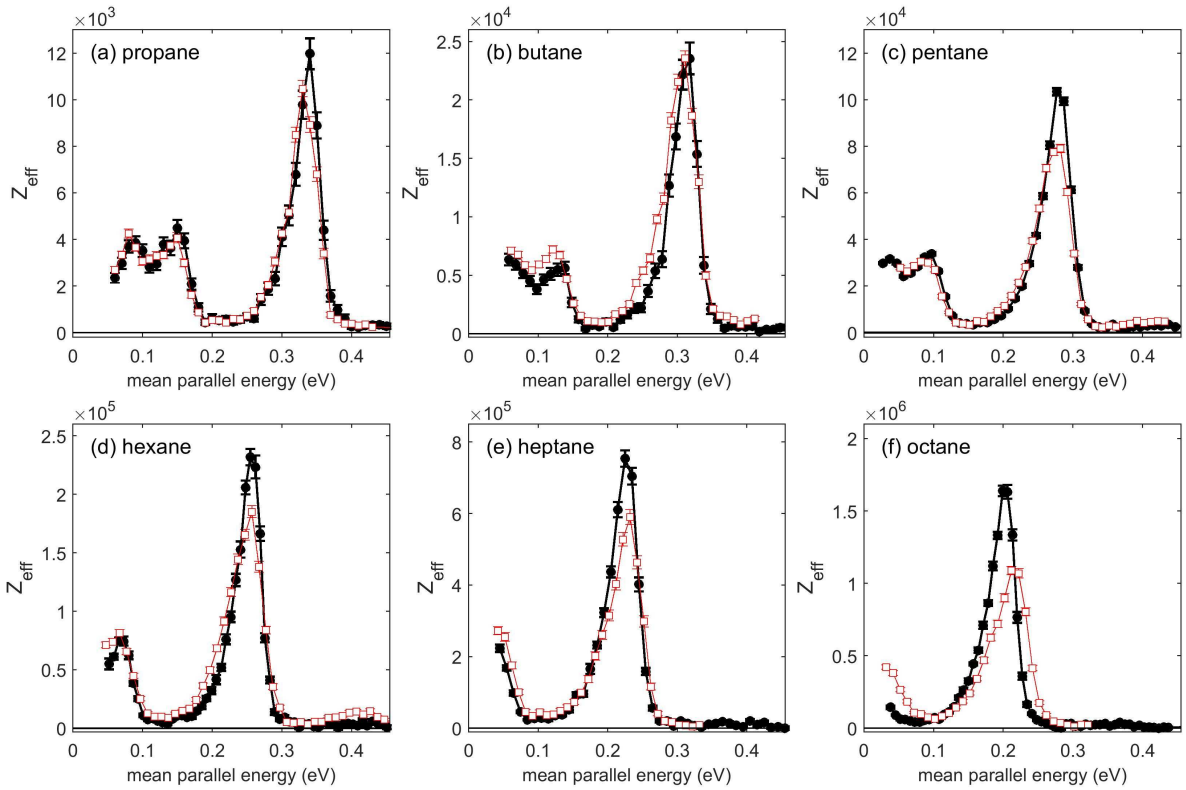

FIG. 6. New $Z_{\rm eff}$ spectra (solid circles) for linear alkanes compared to previous spectra (open squares) from Ref. [7], shifted by 24 meV. See the text for details. Lines connect the data points and are only guides.

to an average C-H stretch vibrational mode energy, which was kept fixed for all molecules [8]. In this procedure, the asymmetric nature of the C-H stretch peak was essentially ignored beyond accounting for the mean perpendicular energy as described above.

However, as shown by the VFR theory of Ref. [1], the peak of the total energy distribution does not occur at the mean total energy (c.f. Fig. 2(c)). This can be corrected by shifting the energy scale to give the proper mean parallel energy of the beam as it exits the BGT, and then using the EMG function with the measured beam parameters to analyze the spectrum. In this way, the proper mean-to-peak shift is included.

In addition, in the previous analysis, only a single approximate C-H mode energy was considered, and the different vibrational modes for the various molecules were not taken into account. Since each molecule is different, the difference between the old and new values of $\varepsilon_{\rm B}$ varies depending on the specific details of the modes. In some cases, the difference is negligible, while in other cases, it can account for as much as 5 meV.

To check the consistency between the two data sets, the energy scales for propane through octane from Ref. [7] were shifted down by 24 meV. This includes 25 meV to obtain the proper mean parallel energy, but then subtracts 1 meV to account for the change in the perpendiucular energy between the two data sets. The resulting spectra are shown in Fig. 6 along with the new data sets. No additional scaling to $Z_{\rm eff}$ was included, so these are absolute comparisons. As can be seen, with the exception of octane, the agreement of the energy scales between the two data sets is quite good. Further, except for the peak magnitude of the high-energy C-H resonances in the larger molecules, the magnitude and shape of most of the spectra are in good agreement.

For pentane through octane, the assumption is that the primary difference in the magnitude of the C-H peaks is due to SCA miscounting at high count rates. Further, as discussed above, the average energy of each successive beam pulse is not constant; since the older experiments used multiple bounces in the counting window, a broadening and slight shift of the spectrum would be expected. An example of this is shown in Fig. 3 for data taken near the peak of $Z_{\rm eff}$. The next bounce has a slight drop in the peak height, and then the third bounce has a larger drop. Since as discussed above, the mean en-

ergy of each bounce is slightly higher, the subsequent bounces are lifted to higher energy and *away* from the resonance, leading to diminished signal. This is not due to elastic scattering since it maintains the total energy and the resonance depends on only the total energy of the positron. This also explains why the change in the magnetic field (in the old data runs) did not change the shape of the measured resonance. A change in the magnetic field will shift the mean of the parallel energy, but will not affect the total energy distribution, and hence will not affect the shape of the resonance.

The one major outlier is the older data set for octane shown in Fig. 6(f) [7]. There is an extra ~ 10 meV difference in ε_B between the data sets that is not understood. Future high-resolution studies with the CBT will allow for a further check on the octane measurement.

VI. RESULTS FOR OTHER ALKANES

A similar incorrect shift of the energy scale was used as the basis for the previous analyses for other molecules studied including ethane, nonane, decane, dodecane, tetradecane, and hexadecane [7–9, 34]. The results are shown with an asterisk in Table I. For most of the large molecules, the C-H stretch peak was attenuated due to miscounting. However, as above, the high-energy edge combined with the shape of the beam distribution provides a lower bound on ε_B. Further, the number of IR active modes, and their spread in energy, becomes larger for the larger molecules; thus the peak is broader and the effect of miscounting on ε_B will be somewhat diminished. Given these considerations, the uncertainties for these molecules are higher than those for other molecules in Table I.

The correction procedure described above resolves a previous mystery associated with the binding energy of ethane [7]. Although ethane shows evidence of VFR (which requires binding), the C-H peak occured at an energy *above* that of the vibrational mode energy (i.e., a value for which a VFR is not possible). With the corrections described above, the VFR peak in ethane lies below the C-H mode energy. This resolves the previous contradiction, and results in an estimate of ε_B for ethane of 3 ± 3 meV. Unfortunately, the precise value is undetermined due to the large error bar.

In the largest alkanes, the corrections described above result in smaller changes in ε_B. This is because, in the new analysis, the focus is on the high energy edges of the VFRs, but combined with convolutions with all IR-active modes. For the larger molecules, these two effects tend cancel, and so the overall change to the quoted value is typically comparable to the error bars. The corrections to ε_B for the second bound states are similarly modest.

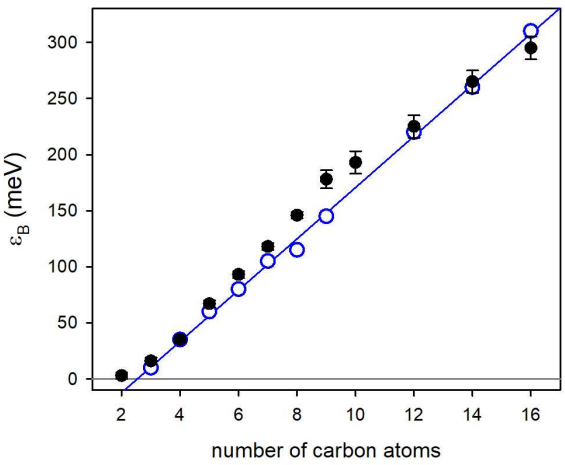

FIG. 7. Corrected values of positron binding energies for the linear chain alkanes (solid circles, •) are shown vs the number of carbon atoms and compared to previously reported values (open circles, ○) [8, 9]. The previous linear relationship is shown by the solid line [3, 8].

New values for the entire data set are compared to the previous measurements in Fig. 7. Also shown is the original linear relationship of ε_B to the number of carbons [8]. Later, using the polarizability instead of number of carbons, a simple linear fit formula was obtained with $\varepsilon_B(\text{meV}) = 12.4\,(\alpha - 5.6)$ [3]. Measurements for butane to octane still show an approximately linear increase with the number of carbon atoms; however, the slope is slightly larger than for the previous measurements. Further, as can be seen from the corrected data, the linear increase bends to a smaller slope between nonane and decane, resulting in a weaker slope for the largest molecules studied.

This change in slope for larger alkanes was originally predicted by Gribakin and Lee using a zero-range-potential model to calculate ε_B [35]. The inability to reproduce the linear slope in the data provided the motivation for many studies that followed.

More recent model-potential calculations, which include the full molecular geometry, also show the same weaker slope for larger numbers of carbon atoms [15]. The new reported values for ε_B in Table I are compared to the calculations in Fig. 8. Values for the second bound states are also shown. Given that the model calculations require only two parameters, the agreement with the experimental measurements is quite good, although the predicted ε_B values for the two largest alkanes are slightly smaller (larger) than the measurements for the first (second)

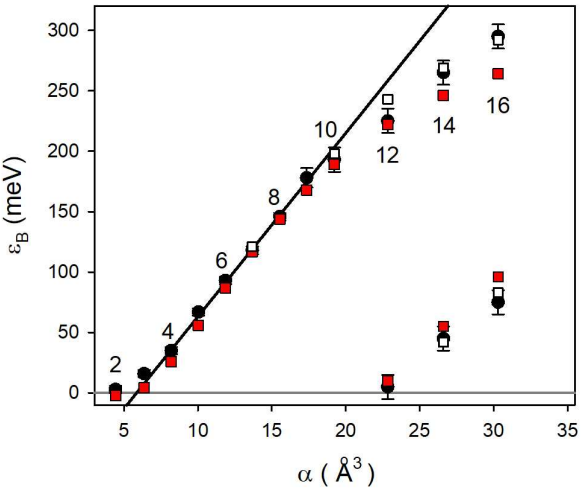

FIG. 8. New and corrected ε_B values for the linear alkanes (solid circles) plotted against molecular polarizability, including data for second bound states. They are compared with model-potential calculations ε_B(SG) (solid red squares), and the thermal average over conformers $\varepsilon_B(300)$ (open squares). The number of carbon atoms on the molecules is indicated. The solid line shows the measured, approximately linear relationship for butane to nonane, $\varepsilon_B(\text{meV}) = 15.2\,(\alpha - 5.8)$.

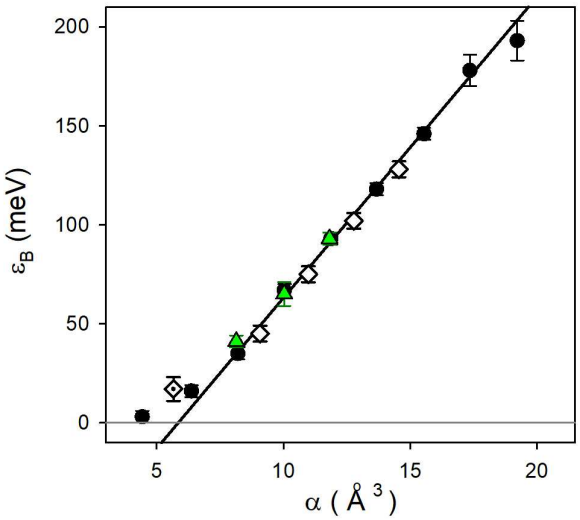

FIG. 9. Binding energies from Table I for saturated alkanes: chain alkanes (solid circles), cycloalkanes (open diamonds), and alkane isomers (green triangles). The solid line is the same as in Fig. 8. The dotted diamond is corrected value for cyclopropane.

bound states. For the molecules butane to nonane, there still is an approximately linear relationship, $\varepsilon_B(\text{meV}) = (15.2 \pm 0.3)\,(\alpha - 5.8 \pm 0.3)$, and this is shown as the solid line in Fig. 8.

For the larger molecules, it is known that there are many conformers possible at room temperature. This raises a question as to whether the different conformers have different ε_B. Swann and Gribakin calculated the ensemble average of ε_B to include the conformers, and the results are listed in Table I as $\varepsilon_B(300)$ [16], and plotted as open squares in Fig. 8. The result is that the linear chain has the *smallest* ε_B, and all of the conformers, being more compact, show varying increases in binding [16]. Thus, the average over the ensemble is predicted to *increase* ε_B, in agreement with the corrected measurements. In contrast, they found that the second bound state has the *highest* ε_B compared with the conformers, again in agreement with the corrected measurements. The results indicate that the inclusion of conformers makes a significant contribution to the measured ε_B for these molecules. The implications of these results would benefit from further theoretical and experimental investigation.

VII. COMPARISON OF ALKANE RINGS, CHAINS AND ISOMERS

Binding energies for chain alkane molecules, cycloalkanes and several branched isomers are compared in Table I [20, 32], and this expanded data set is shown in Fig. 9 as a function of molecular polarizability. For these saturated alkanes (i.e., all with single bonds), the major difference is the number of methyl (CH_3) or methylene (CH_2) groups. The ring molecules have only methylene groups, whereas the n-chains have two additional methyl groups (one at each end), and the branched isomers have varying numbers of each group.

The molecular polarizability is determined predominantly by the number of C and H atoms and is approximately the same for different isomers. For all molecules shown in Fig. 9, the dipole moment is small (< 0.5 D) and is not expected to play a large role in determining ε_B. Thus, it is expected that the binding energy will be roughly similar for similarly sized molecules as shown in Fig. 9.

The measured binding energies for cycloalkanes can be compared to the model-potential calculations of Ref. [16] (which did not consider averaging over conformers). The results are shown in Fig. 10. Good agreement is seen for molecules smaller than cyclooctane, but there are discrepancies for larger molecules. This is presently not understood and is thus worthy of further scrutiny.

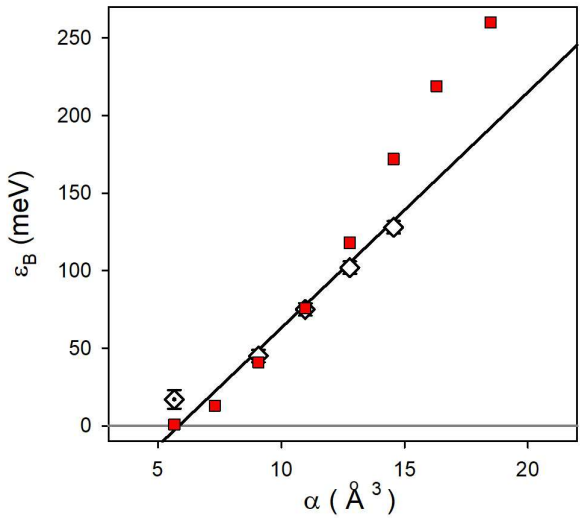

FIG. 10. New and corrected values for ε_B for ring alkanes (open diamonds) plotted against the molecular polarizability. They are compared to model-potential calculations of Ref. [16] (solid red squares). The solid line is the same as in Fig. 8. The dotted diamond is the corrected value for cyclopropane.

VIII. SUMMARY AND CONCLUDING REMARKS

New annihilation spectra were presented for the alkane molecules propane through octane. They depend on the total energy distribution of the beam and requires knowledge of all of the beam properties. It was shown that use of the adiabatic invariant allows for measurement of the complete beam distribution necessary to properly fit the asymmetric peaks in the spectra. The new spectra were used to identify and address systematic errors present in the previous analysis, and to provide updated values of ε_B for all alkanes measured to date. These positron-molecule binding energy measurements represent the most detailed study of this kind for any chemical species. As such, they provide an important test of our understanding of positron-molecule binding energies and Feshbach-resonant annihilation rate amplitudes.

In the course of this reanalysis, previous issues regarding alkane annihilation spectra were resolved. Corrected data for ethane, which exhibits VFR, is shown to likely have a positive binding energy, in contrast to the results of the earlier analysis. In addition, the approximately linear trend of increasing ε_B with increasing molecular size, which was observed in the early measurements, was shown to be valid only for the smaller alkanes. As the size of the molecule increases, ε_B is observed to become a weaker function of the size, in generally good agreement with the recent model-potential calculations of Swann and Gribakin [15, 19]. Further, it was shown that conformers play a measurable role in setting ε_B values for measurements using 300 K gases. A thermal average over multiple molecular conformers needs to be included in order to achieve better quantitative agreement with the measurements of ε_B values of the first and second bound states for the largest alkanes.

More generally, the convergence of more precise experimental measurements with *ab-initio* positron-molecule binding energy calculations for small molecules [18, 36, 37] and model-potential calculations for larger ones [15, 17, 19], has resulted in improved confidence in the theory and in important physical insights. One such recent discovery is that molecules with π bonds have markedly different annihilation spectra and ε_B values [18, 21] than the single-bonded molecular species considered here (e.g., aromatic molecules compared to the cycloalkanes). This raises a number of questions yet to be addressed. For example, both the addition of π bonds and the addition of large dipole moments have separately been shown to enhance ε_B [21, 38]. However, it is not clear how the two effects will change ε_B when both are present in the same molecule (e.g., a substituted aromatic molecule such as benzaldehyde).

Looking to the future, it would be beneficial to study with more precision the larger alkanes, such as hexadecane. Based on the observations for octane, for example, it is likely that the previous measurements had counting errors. Obtaining accurate absolute magnitudes of $Z_{\rm eff}$ for these larger molecules could address the question as to whether there is a maximum possible annihilation amplitude for large-ε_B molecules. Similarly, a new measurement of the smallest chain alkane ethane, using the high-resolution cryo-beam could possibly enable more precise measurements of ε_B for this molecule, even if it is in the sub-5 meV range.

In contrast to the ε_B measurements, our understanding of the *amplitudes* of the annihilation spectra as a function of incident positron energy is at a much less mature stage. A theory of annihilation spectra for dipole-allowed fundamental modes provides insight [1] and can be tested further with improved experimental resolution. The dipole coupling can be obtained from IR spectral measurements; and since high-accuracy IR spectra are available for many alkanes [39–41], these molecules would make an excellent test of the predicted absolute annihilation rates from the VFR theory (and/or possible departures from it). While the theory is known to fail for the high energy C-H stretch mode, its applicability for small molecules and other regions of the

annihilation spectrum is an open question.

Finally, many other spectral features are now known to be present (e.g., possibly combination and overtone VFR) for which a quantitative understanding is lacking [31, 32], although there has been some progress in including higher order mode coupling in the VFR theory [42]. It is hoped that higher resolution annihilation spectra and further theoretical work can shed additional light on this important phenomenon.

ACKNOWLEDGMENTS

We thank G. F. Gribakin, A. Swann, and D. Green for helpful conversations. This work was supported by the U. S. NSF, grant PHY-2010699.

[1] G. F. Gribakin and C. M. R. Lee, Phys. Rev. Lett. **97**, 193201 (2006).
[2] G. F. Gribakin, J. A. Young, and C. M. Surko, Rev. Mod. Phys. **82**, 2557 (2010).
[3] J. R. Danielson, J. A. Young, and C. M. Surko, J. Phys. B **47**, 225209 (2009).
[4] C. M. Surko, A. Passner, M. Leventhal, and F. J. Wysocki, Physical Review Letters **61**, 1831 (1988).
[5] T. Murphy and C. Surko, Physical Review Letters **67**, 2954 (1991).
[6] K. Iwata, R. Greaves, T. Murphy, M. Tinkle, and C. Surko, Physical Review A **51**, 473 (1995).
[7] L. D. Barnes, S. J. Gilbert, and C. M. Surko, Phys. Rev. A **67**, 032706 (2003).
[8] L. Barnes, J. Young, and C. Surko, Physical Review A **74**, 012706 (2006).
[9] J. Young and C. Surko, Physical Review A **77**, 052704 (2008).
[10] G. F. Gribakin and C. M. R. Lee, Eur. Phys. J. D **51**, 51 (2009).
[11] S. J. Gilbert, C. Kurz, R. Greaves, and C. Surko, Applied Physics Letters **70**, 1944 (1997).
[12] S. J. Gilbert, L. Barnes, J. Sullivan, and C. M. Surko, Physical Review Letters **88**, 043201 (2002).
[13] J. R. Danielson, D. H. E. Dubin, R. G. Greaves, and C. M. Surko, Rev. Mod. Phys. **87**, 247 (2015).
[14] S. Ghosh, J. R. Danielson, and C. M. Surko, J. Phys. B **53**, 085701 (2020).
[15] A. R. Swann and G. F. Gribakin, Phys. Rev. Lett. **123**, 113402 (2019).
[16] A. R. Swann and G. F. Gribakin, J. Chem. Phys. **153**, 184311 (2020).
[17] Y. Sugiura, T. Takayanagi, Y. Kita, and M. Tachikawa, Eur. Phys. J. D **73**, 1 (2020).
[18] J. Hofierka, B. Cunningham, C. M. Rawlins, C. H. Patterson, and D. G. Green, Nature **606**, 688 (2022).
[19] A. R. Swann, G. F. Gribakin, J. R. Danielson, S. Ghosh, M. R. Natisin, and C. M. Surko, Phys. Rev. A **104**, 012813 (2021).
[20] J. R. Danielson, S. Ghosh, and C. M. Surko, J. Phys. B **54**, 225201 (2021).
[21] J. R. Danielson, S. Ghosh, and C. M. Surko, Physical Review A **106**, 032811 (2022).
[22] T. J. Murphy and C. M. Surko, Phys. Rev. A , 5696 (1992).
[23] M. R. Natisin, J. R. Danielson, and C. M. Surko, J. Phys. B **47**, 225209 (2014).
[24] M. Natisin, J. Danielson, and C. Surko, Phys. Plasmas **22**, 033501 (2015).
[25] M. R. Natisin, J. R. Danielson, and C. M. Surko, Phys. Plasmas **23**, 023505 (2016).
[26] J. Young and C. Surko, Nuclear Instruments and Methods in Physics Research Section B: Beam Interactions with Materials and Atoms **247**, 147 (2006).
[27] M. R. Natisin, J. R. Danielson, and C. M. Surko, Appl. Phys. Lett. **108**, 024102 (2016).
[28] M. R. Natisin, Ph.D. thesis, University of California, San Diego (2016).
[29] T. Shimanouchi, *Tables of molecular vibrational frequencies*, Vol. 1 (National Bureau of Standards Washington, DC, 1972).
[30] W. E. Wallace, in *NIST Chemistry WebBook, NIST Standard Reference Database Number 69*, edited by P. Linstrom and W. Mallard (National Institute of Standards and Technology, Gaithersburg MD, 20899) Chap. Infrared Spectra.
[31] S. Ghosh, J. R. Danielson, and C. M. Surko, Physical Review Letters **129**, 123401 (2022).
[32] S. Ghosh, J. R. Danielson, and C. M. Surko, Phys. Rev. Lett. **125**, 173401 (2020).
[33] D. R. Lide, ed., *CRC Handbook of Chemistry and Physics*, 89th ed. (CRC Press, 2008-2009).
[34] A. C. L. Jones, J. R. Danielson, M. R. Natisin, C. M. Surko, and G. F. Gribakin, Phys. Rev. Lett. **108**, 093201 (2012).
[35] G. F. Gribakin and C. M. R. Lee, Nuclear Instruments and Methods in Physics Research Section B: Beam Interactions with Materials and Atoms **247**, 31 (2006).
[36] M. Tachikawa, Y. Kita, and R. J. Buenker, Physical Chemistry Chemical Physics **13**, 2701 (2011).
[37] M. Tachikawa, Y. Kita, and R. J. Buenker, New Journal of Physics **14**, 035004 (2012).
[38] J. R. Danielson, A. C. L. Jones, J. J. Gosselin, M. R. Natisin, and C. M. Surko, Phys. Rev. A **85**, 022709 (2012).
[39] T. J. Johnson, L. T. Profeta, R. L. Sams, D. W. Griffith, and R. L. Yokelson, Vibrational Spectroscopy **53**, 97 (2010).
[40] S. D. Williams, T. J. Johnson, S. W. Sharpe, V. Yavelak, R. Oates, and C. S. Brauer, Journal of Quantitative Spectroscopy and Radiative Transfer **129**, 298 (2013).

[41] I. E. Gordon, L. S. Rothman, R. J. Hargreaves, R. Hashemi, E. V. Karlovets, F. M. Skinner, E. K. Conway, C. Hill, R. V. Kochanov, Y. Tan, *et al.*, Journal of quantitative spectroscopy and radiative transfer **277**, 107949 (2022).
[42] G. F. Gribakin, J. F. Stanton, J. R. Danielson, M. R. Natisin, and C. M. Surko, Phys. Rev. A **96**, 062709 (2017).